



# Influence of shape distortion on the precision of holes in parts fabricated by metal binder jetting

M. Zago<sup>1</sup> · N. Lecis<sup>2</sup> · M. Mariani<sup>2</sup> · O. U. Uçak<sup>1</sup> · I. Cristofolini<sup>1</sup>

Received: 29 July 2022 / Accepted: 13 April 2023  
© The Author(s) 2023

## Abstract

Metal binder jetting (MBJ) is an additive manufacturing (AM) technology split into two process steps: printing and sintering. Firstly, product is built up layer-by-layer by the selective deposition of a binder agent on a powder bed. Secondly, a thermal treatment (sintering) consolidates the metal structure. MBJ is currently becoming more and more attractive on the reason of high potential scalability, cost-effective production and wide range of available material feedstocks. However, the transition towards industrial scale production is restrained by the critical control of dimensional and geometrical precision of parts after sintering operation. In fact, product geometry is affected by anisotropic dimensional change or even shape distortion. This study aims at investigating the dimensional and geometrical precision of through holes. Three sample geometries were designed, having a through hole with axis perpendicular to the building direction and located at different levels along sample height. Samples were measured by a coordinate measuring machine before and after sintering, in order to assess the shrinkage and any shape change. Results highlight the inhomogeneous volumetric and linear shrinkage of the three geometries, which is influenced by the printing position in the building plane. A macroscopic deformation of parallelepiped geometry was also evidenced, caused by the superposition of layer shifting originated on printing, and by the frictional forces between sample surface and alumina support during sintering. Such distortion significantly affects the shrinkage and form error of holes.

**Keywords** Metal Binder Jetting · Design for AM · Dimensional and Geometrical Precision · Shape Distortion

## 1 Introduction

Additive manufacturing (AM) has produced a revolution in the conventional design methodology. Complex geometries which are not technically and economically affordable by traditional manufacturing techniques can now be fabricated by AM. Each of the seven AM processes, summarized by ISO/ASTM 52,900:2021, have specific advantages and drawbacks which delineate a potential development in peculiar markets [1]. Therefore, new applications are currently being researched for taking advantage of the opportunities offered by novel design paradigm [2].

Among AM processes, binder jetting (BJ) is currently gaining an increasing attention by research community and

companies, due to the high production rate and low feedstock price. Other advantages consist of the processability of nearly any material feedstock (metal, hard-metal, ceramic powders etc.), with no need for supports during the printing process [3, 4].

Metal binder jetting (MBJ) is a sinter-based additive manufacturing technique, the process splits into two steps: printing and sintering. Basically, a 3D CAD file is processed by slicing algorithms, which generate the instructions for the printing operation. The fabrication of each layer proceeds joining the particles by selective deposition of a liquid bonding agent. Powders are fed by a hopper and the resulting layer thickness is controlled by a blade or a roller, leveling and smoothing the powders deposited in advance. Successively, a printhead scans the building plane and selectively injects a binder agent in correspondence of the section of the CAD product. After binder injection, in some cases a heating source scans the building plane for drying the excess of the liquid binder, which has not been absorbed [5]. Next layers are printed moving down the building plane and repeating the spreading of metal powders and the binder injection. At

✉ M. Zago  
marco.zago-1@unitn.it

<sup>1</sup> Department of Industrial Engineering, University of Trento,  
Via Sommarive 9, 38123 Trento, Italy

<sup>2</sup> Department of Mechanical Engineering, Politecnico di  
Milano, Via Privata La Masa 1, 20156 Milano, Italy

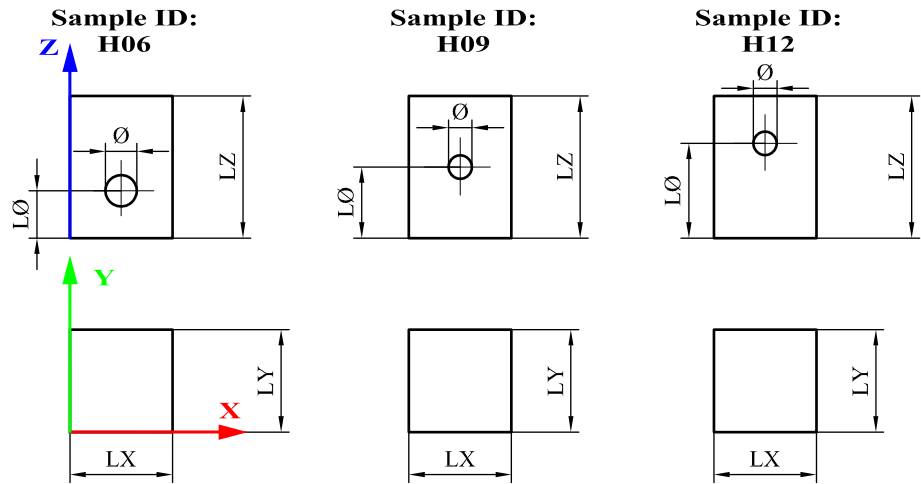
the end of printing procedure, the product cannot be removed from the printing box, since the weak forces between powder particles do not allow safe handling of the printed part. Other treatments are mandatory, namely: curing, de-powdering, de-binding and sintering. The curing operation consists of moving the printing box in a furnace for a thermal treatment between 70 °C and 200 °C for some hours [6]. This step induces a cross-link of the polymeric binder, which slightly increases the part resistance in order to avoid any parts damage during the de-powdering, that is the removal of the excess of powder from the building box and parts extraction. The product is then subjected to two subsequent thermal treatments. The first one is called de-binding, samples are held at an isothermal temperature between 300 and 900 °C to allow binder cracking in volatile compounds [7]. After de-binding, products are heated up at higher temperatures to activate sintering mechanisms, which consolidate the metal structure through the growth of neck contacts between particles, and the consequent closure of porosity.

Sintering has a strong impact on the precision of products, due to the dimensional and shape changes caused by porosity closure and material densification. Literature reports a volumetric shrinkage between 10 and 50% [8], the broad interval depends on the effect of particle size distribution and sintering conditions (time and temperature) [9, 10]. In addition, linear shrinkage is generally higher along building direction than in the building plane, as reported by Lores et al. for several metal powders [6]. Consequently, designers have to properly scale the nominal geometry at the green state in order to compensate the dimensional change on sintering. Hence, the correct tuning of scaling factors is fundamental for controlling the dimensional and geometrical precision of sintered parts.

Nevertheless, the precision of sintered products is also affected by the printing operation. Several papers describe the detrimental effect of layer-by-layer manufacturing. The discretization of surface profile, which is generally called staircase or stair-stepping error, produces discontinuity on the target surface which influences both geometrical features and surface roughness. Some models have been proposed for estimating the effect of building orientation and layer fabrication on flatness [11] and cylindricity form error [12]. Literature generally proposes adaptive slicing approach for minimizing form error and maximizing productivity [13]. However, in metal binder jetting, the staircase error does not completely explain the form error at green state, as experimentally verified in [14]. The un-proper control of printing process can produce bleeding or layer shifting defects. As explained in [15], bleeding is defined as the leak of binder out of nominal contour of the product. This defect can occur by an excessive binder saturation or insufficient drying condition. Cao et al. describe layer-shifting as the alteration of the printed

layer locations, which determines part dragging within powder spreading direction. The layer shifting defect is ascribed to the state of stress and powder failure mechanisms induced by powder spreading [16]. As reported by Huang et al., several parameters affect the dimensional and form error of cylinders, as STL file, slicing (staircase error), and actual printing operation, namely the inhomogeneity in material and process control [17]. Some experimental work studied the precision of binder jetting products at the green state. Islam and Sacks did not observe a trend between nominal size and dimensional error of multiple concentric cylinders [18]. Ollison and Berisso highlighted a higher influence of inclination angle than diameter size on the cylindricity form error [19]. Dahmen et al. compared the precision of holes in parts fabricated by MBJ and laser powder bed fusion (L-PBF) by the analysis of images acquired by X-ray computed tomography. Their research shows that the deviation from nominal size and shape of holes in parts produced by MBJ is poorly affected by the inclination in comparison to the same feature produced by L-PBF [20].

In previous work the dimensional and geometrical precision of through holes having different diameter size and inclined at different orientation with respect to the building direction have been studied [21, 22]. An analytical model for predicting the diameter shrinkage and circularity form error caused by the anisotropic shrinkage has been successfully tested. The model can capture the empirical trend of cylindricity form error and shrinkage at different inclination of hole axis, however some discrepancies have been observed for smallest holes (3 mm diameter), when hole axis is perpendicular to the building direction. The marked underestimation of the experimental results has been ascribed to the combined effect of viscous-plastic material behavior and gravity load, on the basis of previous experimental work on shape deformation of overhanging structure and cantilever beams [23–25]. It was supposed that the mass of powder above hole section might have determined an extra deformation of hole section, on the reason of viscous-plastic material behavior. This work aims at investigating the dimensional and geometrical precision of through holes in parts fabricated by metal binder jetting process, being the prediction of hole shrinkage and deformation crucial for the development of a robust design approach. Specifically, this study aims at studying holes perpendicular to the building direction, in order to comprehend the discrepancy observed in the previous work. The holes were designed at three height levels in order to verify the effect of different gravity load related to the mass of powder on the hole section. Samples were then measured by a coordinate measuring machine before and after sintering, in order to assess the actual dimensional change of linear dimensions and diameter. In addition, form error is analyzed and compared with the analytical model proposed in the previous work.

**Fig. 1** Geometry and dimensions IDs of samples investigated**Table 1** Nominal dimensions of the three geometries

Geometry	Nominal dimensions				
	LX (mm)	LY (mm)	LZ (mm)	$\phi$ (mm)	$L\phi$ (mm)
H06	13	13	18	3	6
H09	13	13	18	3	9
H12	13	13	18	3	12

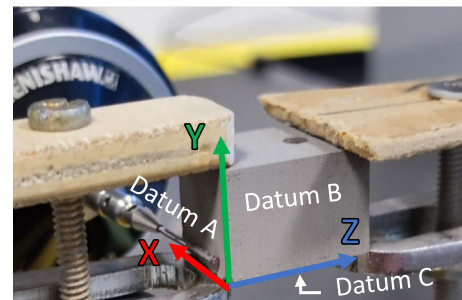
## 2 Materials and methods

This work aims at experimentally investigating the precision of through holes, which are located at different height levels with respect to the building plane. Parallelepiped samples were designed having a single through hole of 3 mm, whose axis is parallel to the building plane. Three geometries were modelled, differing for the position of the hole's axis as shown in Fig. 1, whereas nominal dimensions are reported in Table 1. According to the reference system depicted in Fig. 1, hole axis is aligned with Y direction, which corresponds to the printhead movement in the building machine. X direction corresponds to the powder spreading direction. According to the hole position, sample geometries are named: H06, H09 and H12.

For each geometry, three replicates were fabricated by ExOne Innovent Plus machine. All samples were printed in the same batch in order to minimize process variability. The replicates were randomly distributed in the building plane with the scope of highlighting any possible influence of the printing position as observed by Vitolo et al. in [26].

Samples were fabricated by 316L metal powders with a particle size distribution of D90 25  $\mu\text{m}$ , D50 10  $\mu\text{m}$  and D10 4  $\mu\text{m}$ , according to Sandvik AM (Sweden) supplier. Printing parameters were set-up according to the optimization study described in [7] and the values are reported in Table 2.

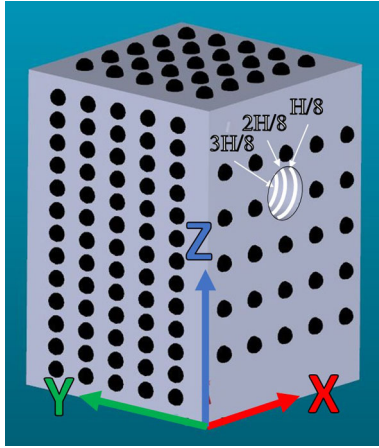
After curing and de-powdering, green parts were measured by means of a Global DEA coordinate measuring

**Fig. 2** Constrain set-up and datum reference frame

machine (CMM), with a maximum permissible error of  $1.5 + L/333 \mu\text{m}$ , in accordance with ISO 10360-2. As shown in Fig. 2, samples were carefully constrained aiming at maximizing the surface reachable by the probe. The measurement procedure firstly identified the datum reference frame. According to the reference frame indicated in Fig. 2 (same as the reference frame in the printing chamber, as shown in Fig. 1), four points were acquired on the plane XY, which corresponds to the first printed layer. The points were then fitted by a least-squares algorithm and the reconstructed plane was associated to the first datum plane (Datum A), which defines the orientation of Z axis and the Z origin. After that, planes YZ and XZ were reconstructed by four points according to the same procedure. The second datum plane (Datum B) identifies the X axis and the X origin. Finally, third Y origin is determined by the Datum plane C (plane XZ).

**Table 2** Printing process parameters

Layer thickness ( $\mu\text{m}$ )	Saturation level (%)	Bed temperature ( $^{\circ}\text{C}$ )	Drying time (s)	Recoater speed (mm/s)	Roller rotation speed (rpm)	Roller transverse speed (mm/s)
50	55	55	12	100	600	5

**Fig. 3** Location of points used for the reconstruction of planes and holes (at seven depth levels, from  $H/8$  to  $7H/8$ )

After the definition of the datum reference frame (DRF), the measurement routine proceeded acquiring four points on each surface and reconstructing planes A2, B2 and C2 by the best fit least squares method. Hence, the linear dimensions can be computed as the distance of opposite planes. These dimensions were then used for a more accurate measurement. As shown in Fig. 3, 25 points were successively acquired on planes A and A2 (opposite to plane A), 65 on planes B and B2 and 24 on planes C and C2. The coordinates of each point were parametrically defined as a fraction of the approximate linear dimensions previously computed. The X and Y coordinates of points on planes A and A2 range from  $1/6$  to  $5/6$  of the measured linear dimensions on X and Y directions. Same, the coordinates of points on planes B and B2 were located fractioning Y and Z dimensions, by  $1/6$  and  $1/14$ , respectively. Same strategy was adopted for points on planes C and C2, taking into account the presence of clamping system. This approach allows a more precise reconstruction of surfaces due to the higher number of points acquired. Therefore, DRF has been re-defined by the new reconstructed planes A, B and C. Furthermore, this measurement strategy allows a coherent measurement of sintered samples, being the coordinates of points parametrized as function of an approximate estimation of sample dimensions, thus reliably identified even in case of high-volume change after sintering. Finally, the parametric definition of points coordinates permits the acquisition of the points in the same position both at green and sintered state.

The hole was inspected at 7 depth levels, equally spaced along the through hole as shown in Fig. 3. At each level, 24 points were acquired on the circumference. The circle was then reconstructed by a best-fit least squares method, also identifying the X and Y coordinates of the circle center.

After measurement, green parts were de-binded at  $470^{\circ}\text{C}$  for 4 h in Argon atmosphere and successively sintered in a vacuum furnace ( $10^{-1}$  mbar) at the isothermal sintering temperature of  $1360^{\circ}\text{C}$  for 3 h. Sintered samples were measured according to the same measurement routine defined for green parts.

Dimensional change on sintering was computed by Eqs. (1) and (2), for linear dimensions and diameter, respectively.

$$\varepsilon_L = \frac{L_s - L_g}{L_g} \quad (1)$$

$$\varepsilon_\phi = \frac{\phi_s - \phi_g}{\phi_g} \quad (2)$$

where:

- L, represents the linear dimension computed by the distance between opposite planes
- $\phi$ , represents the diameter of the cylinder reconstructed by the circles acquired at seven depth levels in the hole
- g, s subscripts correspond to the green and sintered state, respectively.

Volumetric shrinkage ( $\varepsilon_V$ ) was expressed by Eq. (3), where volume was calculated by the difference between the volume of parallelepiped and the cylindrical hole derived by the measurements.

$$\varepsilon_V = \frac{V_s - V_g}{V_g} \quad (3)$$

The diameter shrinkage was then compared with the analytical model presented in [21] and expressed by Eq. (4)

$$\varepsilon_{\phi-model} = \frac{\sqrt{A}}{2\pi} \int_0^{2\pi} \sqrt{1 - \frac{(A-B)}{A} \sin^2 \alpha} d\alpha - 1 \quad (4)$$

where:

$$A = [(\varepsilon_Y + 1)^2 \cos^2 \theta_g + (\varepsilon_z + 1)^2 \sin^2 \theta_g] \quad (5)$$

$$B = (\varepsilon_X + 1)^2 \quad (6)$$

And:

- $\varepsilon_X$ ,  $\varepsilon_Y$ ,  $\varepsilon_Z$  represent the linear shrinkages along X, Y and Z directions
- $\theta_g$  represents the inclination angle of hole axis with respect to the building direction ( $90^\circ$  in this study)
- $\alpha$  represents a parametric angular coordinate, which ranges between 0 and  $2\pi$ .

The precision of hole was evaluated by circularity and cylindricity form errors. The empirical data were successively compared with the result of Eq. (7).

$$\text{circularity error} = \frac{1}{2} D'_g \left\{ (\varepsilon_X + 1) - \sqrt{[(\varepsilon_Y + 1)^2 \cos^2 \theta_g + (\varepsilon_Z + 1)^2 \sin^2 \theta_g]} \right\} \quad (7)$$

where  $D'_g$  is the nominal diameter of the circle at the green state.

### 3 Results and discussion

In the next sections the experimental results are discussed with relation to the prevision of the model. The first part presents the anisotropic dimensional change on sintering of linear dimensions. In the second section, the diameter shrinkage of the cylinder is compared with the result of the analytical model. In addition, circularity and cylindricity form errors are analyzed. In the last section, the shape distortion of the parallelepiped sample is shown through the shape of surfaces derived by measured points, and the local shrinkage is obtained by the point-by-point distance acquired on opposite faces.

#### 3.1 Dimensional change on sintering of linear dimensions

Figure 4 shows the significantly anisotropic linear shrinkage on sintering. This result corroborates the markedly higher shrinkage of sample height (LZ), compared to dimensional changes in the printing plane, shown in several studies [7, 21, 27].

The higher shrinkage along building direction is attributed to the powder rearrangement during de-binding, likely due to the binder decomposition, which in turn provokes an increase of porosity, reducing the powder cohesion. Therefore, gravity load might induce the rearrangement of powders, which

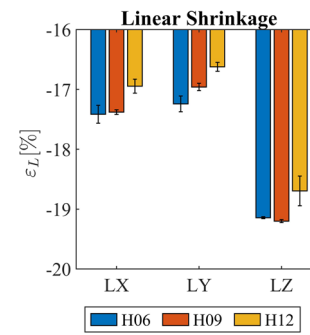


**Fig. 4** Linear shrinkage on sintering of the three sample geometries (H06, H09 and H12). Error bar represents 1sigma distribution of the measurements

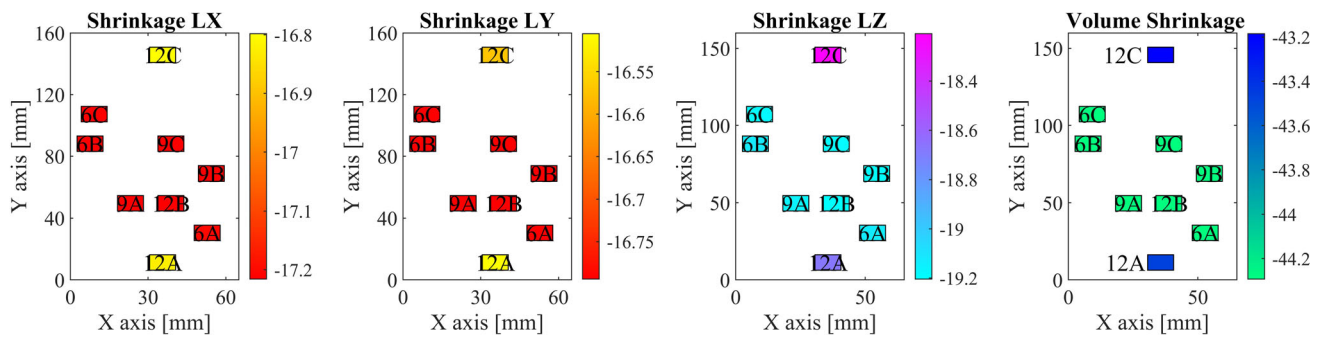
increases the packing factor along building direction (Z direction), and decreases the sample height before the activation of the sintering mechanisms. Another theory was proposed by Wakai in [28]. In this work, a microscopic model was presented, attributing the origin of anisotropic shrinkage to the particle rearrangement produced by the creation of new contacts between powders and the consequent change of sintering force, driving a higher shrinkage along Z direction. Both mechanisms may contribute to shrinking, future studies should clarify the predominant one for better comprehending the phenomena and give the foundation to model theory.

Figure 4 shows that linear shrinkages are not completely homogeneous in the building plane. In fact, a slightly higher shrinkage occurred along printhead movement direction (LX) with respect to the powder spreading direction (LY). Same results have been observed on other works [21, 29], while elsewhere opposite behavior was described [7, 27, 30]. The slightly different shrinkage in the building plane (X–Y plane) might be ascribed to an inhomogeneity of powder distribution or binder saturation. Both phenomena could be directly associated to powder and binder spreading, respectively. This variation of the printing conditions could lead to slight differences of local green density, which successively turn into a different dimensional change on sintering, as observed.

Figure 4 also reveals an appreciably lower shrinkage of samples H12 in the three directions, compared to the other two geometries. Figure 5 shows the position of samples in the printing plane, which might be related to such discrepancy.

Figure 5 shows the linear shrinkage along X, Y and Z directions of each sample according to their position in the building plane, along with the volumetric shrinkage calculated by Eq. (3). Data demonstrate a considerably lower shrinkage of samples 12A and 12C along all directions, by contrast the shrinkage of sample 12B, which was fabricated in the center of the building plane, is in line with other sample geometries. On the basis of such information, it might





**Fig. 5** Linear and volumetric shrinkage of each sample on the basis of sample location in the printing plane

be concluded that printing location has a considerably high influence on the dimensional change on sintering.

Green density inhomogeneity in the building plane is highlighted in the literature by Lores et al. [31]. Do et al. described a decrease of powder bed density at the increase of X coordinate. This behavior is provoked by the decrease of compaction ratio along the movement of the powder roller [32]. Binder injection might reasonably influence green density along the movement direction of the printhead (Y axis), whereas powder spreading could have an effect along movement direction of the recoater (X axis).

Other work numerically analyzed the influence of initial density on densification and sintering shrinkage. Chen et al. investigated by finite-element approach the sintering behavior of cubic samples having a relative density of 49.5%, 51.5% and 53.5% at green state. The simulation provides final sintering density of 94.1%, 96.5% and 98.7%, respectively. The simulation results are in good agreement with the density experimentally measured by Archimedes' test. Hence, it is possible to conclude that densification increases with the increase of initial density, by contrast the shrinkage decreases as the initial density increases [33].

A variation of green density along printhead movement direction is not directly reported in literature. However, the influence of binder saturation is well-known. Lecis et al. report higher dimensional change on sintering on reducing binder saturation [7]. The lower volumetric shrinkage observed in the extreme of Y axis is likely due to the presence of boundary effects, slight variations of the amount of binder injected corresponding to the start and end of the printhead movement pathway. Moreover, powder spreading process could lead to inhomogeneous distribution close to the boundary. Further investigation will verify such hypotheses, through a systematic analysis of the variability of green density.

In conclusion, an accurate knowledge of the linear dimensional change on sintering is mandatory for the correct identification of the scaling factor to be applied in the CAD file. A higher shrinkage along building direction (Z) with respect to the shrinkage in the building plane (X–Y) has

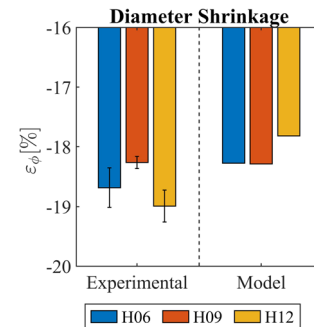


**Fig. 6** Comparison of experimental and predicted diameter shrinkage

been highlighted, as well as a slight difference of dimensional change along powder and binder spreading directions (X and Y). In addition, a non-constant shrinkage was observed in the three geometries on the reason of the influence of sample position in the building plane. Further studies will investigate the green density as function of the position in the building plane and the repeatability of process conditions. This would help designers at correctly scaling the CAD file on the basis of the expected dimensional changes on sintering.

### 3.2 Dimensional change on sintering of diameter

Figure 6 shows the diameter shrinkage of holes located at the three height levels. The experimental data reveal a significant minimum of diameter shrinkage at the intermediate height (H09). In order to comprehend such result, Fig. 6 also reports the diameter shrinkage computed by Eq. (4), which estimates the diameter shrinkage on the basis of the linear dimensional changes LX and LZ shown in Fig. 4.

A good overlap of the empirical data and model prevision can be observed at the intermediate height, whereas model significantly underestimates the dimensional change for holes at lower and higher position. In the previous work [21], the underestimation of the model was supposed to be ascribed to the influence of gravity-induced load of the mass of powder over hole section. The mass of powder could theoretically produce a shape distortion of the hole section on

the reason of the viscous-plastic material behavior of the powder during sintering, in addition to the anisotropic linear shrinkage. This effect might reasonably contribute to the offset observed in the geometry H06, nevertheless there is no evidence of a relationship between hole shrinkage and the mass of powder over the hole. In fact, the higher discrepancy between model and empirical data is observed for the hole located at the higher level (H12), which should be less affected by gravity-induced deformation according to this explanation.

The dimensional change of hole is investigated more in depth in Fig. 7a–c, where histograms report the diameter shrinkage at seven depth levels (depth level increases moving toward the Y direction, as shown in Fig. 3), along with the diameter shrinkage of the reconstructed cylinder (Cyl, black bar) and the model prevision (M, red bar). Results evidence a decreasing shrinkage towards Y direction. Moreover, standard deviation increases on increasing diameter shrinkage for all the geometries. This trend is less evident for the intermediate geometry H09 which shows the higher agreement with the shrinkage prediction, as highlighted above.

The trend of standard deviation and shrinkage can be related to the shape error of the hole. Figure 8 shows the circularity form error measured at the seven depth levels, along with the cylindricity form error and the prevision of form error computed by Eq. (7). Comparing Figs. 7 and 8, the deviation from model prevision is similar.

For the three geometries, the form error and shrinkage are virtually constant from scans 7H/8 to 4H/8, then significantly increase. Therefore, hole shrinkage and form error are similarly affected by shape deformation on sintering. Considering the cylindricity form error, the measured values are not affected by the position of hole axis. Similar results were observed by Dahmen in [20], fabricating holes of 2 mm by the same printing machine. The higher cylindricity error, compared to the circularity average error, suggests an increasing deviation in the position of the center of the circles moving through the hole. Both circularity trend and cylindricity do not fit the prevision of Eq. (7), thus meaning that the anisotropic shrinkage along X and Z direction partially contributed to the origin of form error, but it is not the main cause.

The analysis of circularity form error at the green state reveals the influence of printing. In Fig. 9a–c the circularity form error at the green state is subtracted from the circularity form error at the sintered state. In this way the lack of precision of green parts is considered, so that an improvement is shown comparing the empirical measurements and model prevision. The remaining discrepancies will be clarified on the basis of the analysis presented in the next paragraph.

The analysis above highlighted two main results. First, the hole shrinkage markedly exceeds model prevision in two of the three geometries. Therefore, scaling the CAD geometry

by the linear dimensional change on sintering is not sufficient for controlling hole shrinkage. This aspect is also underlined by the gradient of diameter shrinkage through the hole, which introduces an additional complication in the geometry compensation. Secondly, the circularity and cylindricity form errors are significantly higher than model prevision. The main reason has been attributed to the pre-existing form error at the green state as shown in Fig. 9. Nevertheless, form errors are considerably higher than expected; next section further investigates possible reasons for the discrepancies above highlighted.

### 3.3 Shape distortion

Figure 10a–f plots the front (view X–Z) and side (view Y–Z) view of each of the three samples geometries. In addition to the nominal sintered geometry, the points acquired by CMM are shown. In the front view (view X–Z) the dots represent the projection of the points acquired in the plane B (left dots) and plane B2 (right dots), whereas in the side view (view Y–Z) the dots represent the projection of the points measured in the plane C (left dots) and C2 (right dots).

In all the geometries data show a shift of the points acquired in the planes B and B2 towards X direction on increasing Z coordinate. The repeatability of the observation suggests a process induced phenomenon. In a previous work, layer shifting was observed at the green state [14], and the reason has been ascribed to the powder spreading operation. An interpretation has been proposed by Maximenko et al., who simulated the influence of the powder spreading on the accuracy of layer fabrication [34]. In another work Cao et al. demonstrate a correlation between flatness form error and compaction thickness [16]. The movement of the roller creates a state of stress, determining powder compaction and an increase of green density, as well as deformation of the sample shape, due to the low shear strength resistance before the curing treatment.

In addition to the shape deformation produced by powder spreading, an inhomogeneous surface deformation can be highlighted in the side view (Y–Z). For all the geometries the side view shows a trapezoidal shape outlined by the points measured in the planes C and C2. The same shape was observed by Olevsky and German in [35], simulating the sintering deformation of a cylinder under the effect of gravity load. In their work, by the hypothesis of a viscous-elastic constitutive model, the gravity load produces an increase of the size in the opposite direction with respect to the shrinkage induced by sintering mechanisms. The friction of sample surface with support plate might have also appreciably contributed to the shape deformation. In the case at study, samples were positioned in the sintering furnace on plates made of pure alumina. Hence, frictional forces can raise during sample shrinkage, acting against the material

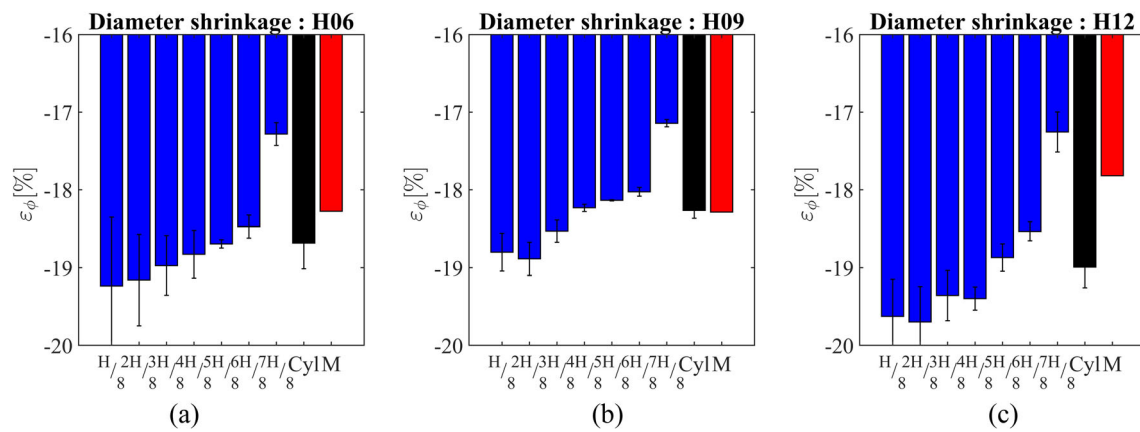


**Fig. 7** Diameter shrinkage of: the circles measured at 7 depth levels, the cylinder, and the model prevision calculated by Eq. (4). **a** geometry H06, **b** geometry H09 and **c** geometry H12

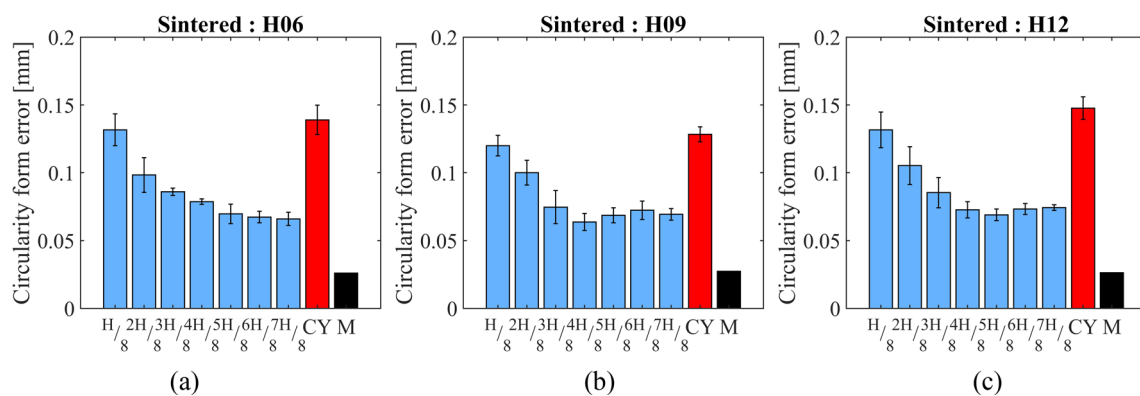


**Fig. 8** Circularity form error measured at the sintered state at different depth levels of the three sample geometries, in addition with cylindricity form error and model prevision computed by Eq. (7). **a** Geometry H06, **b** geometry H09 and **c** geometry H12

densification, and producing a lower linear shrinkage at the basis of sample. Further evidence of the sintering gradient is presented in Fig. 11, which plots the dimensional change on sintering along X and Y direction as calculated by point-by-point distance on the opposite planes. Data demonstrate that the gradient of linear shrinkage along the height occurs both along X and Y directions.

The above analysis highlights a macroscopic deviation from the nominal parallelepiped geometry, certainly affecting the geometry of the holes too, and complicating the possibility of reliably measuring such deformation. The planes measured on the sintered parts for defining the Datum Reference Frame, as described in the measurement procedure, are not strictly orthogonal. Consequently, the actual straightness and orientation of the axes of holes might be not properly identified according to the DRF, and the measurement of circles not strictly performed in correspondence to the actual cylinder section.

The deformation of holes is thus likely related to a deflection of cylinder axis, resulting from the whole macroscopic deformation, rather than to a deviation from circular section.

Such result highlights the criticality of using a measuring method developed for products fabricated by conventional technologies (milling, turning), not determining such high distortion.

As a consequence, the discrepancy between the experimental data and the model prevision plots in Figs. 7 and 9 must be re-considered on the basis of the shape distortion of planes. The compensation of macroscopic geometrical error must precede the compensation of hole dimension and geometry. Future studies will design new sample geometry modified by a counter-deformation corrective function to compensate the boundary shape deformation. In this way, it will be possible to distinguish any inaccuracy of hole geometry ascribable to macroscopic distortion and to effectively validate the prevision model.

## 4 Conclusions

This work investigated the dimensional and geometrical precision of parallelepiped samples fabricated by metal binder



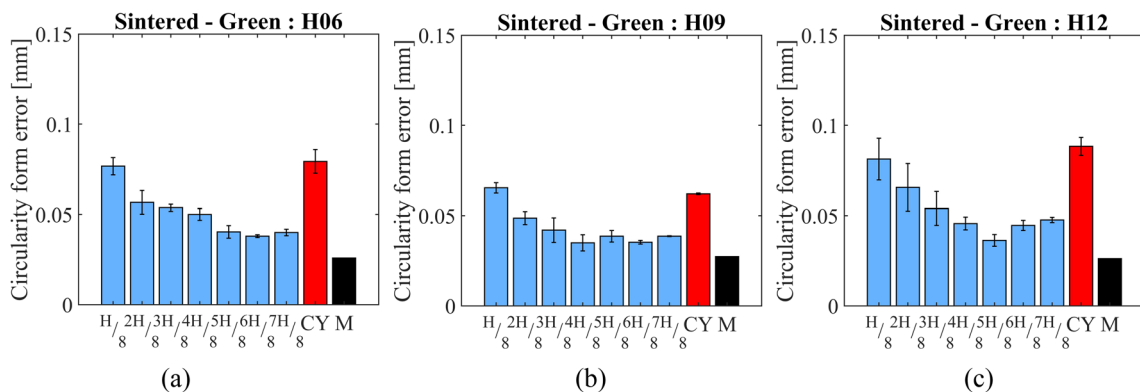


**Fig. 9** Difference between the circularity and cylindricity form error measured at sintered and green state, in addition with model prevision computed by Eq. (7). **a** Geometry H06, **b** geometry H09 and **c** geometry H12

**Fig. 10** Shape distortion of the planes B and B2 (view X-Z) and planes C and C2 (view Y-Z) through the projection of the measured points. **a** geometry H06—view X-Z, **b** geometry H06—view Y-Z, **c** geometry H09—view X-Z, **d** geometry H09—view Y-Z, **e** geometry H12—view X-Z, **f** geometry H12—view Y-Z

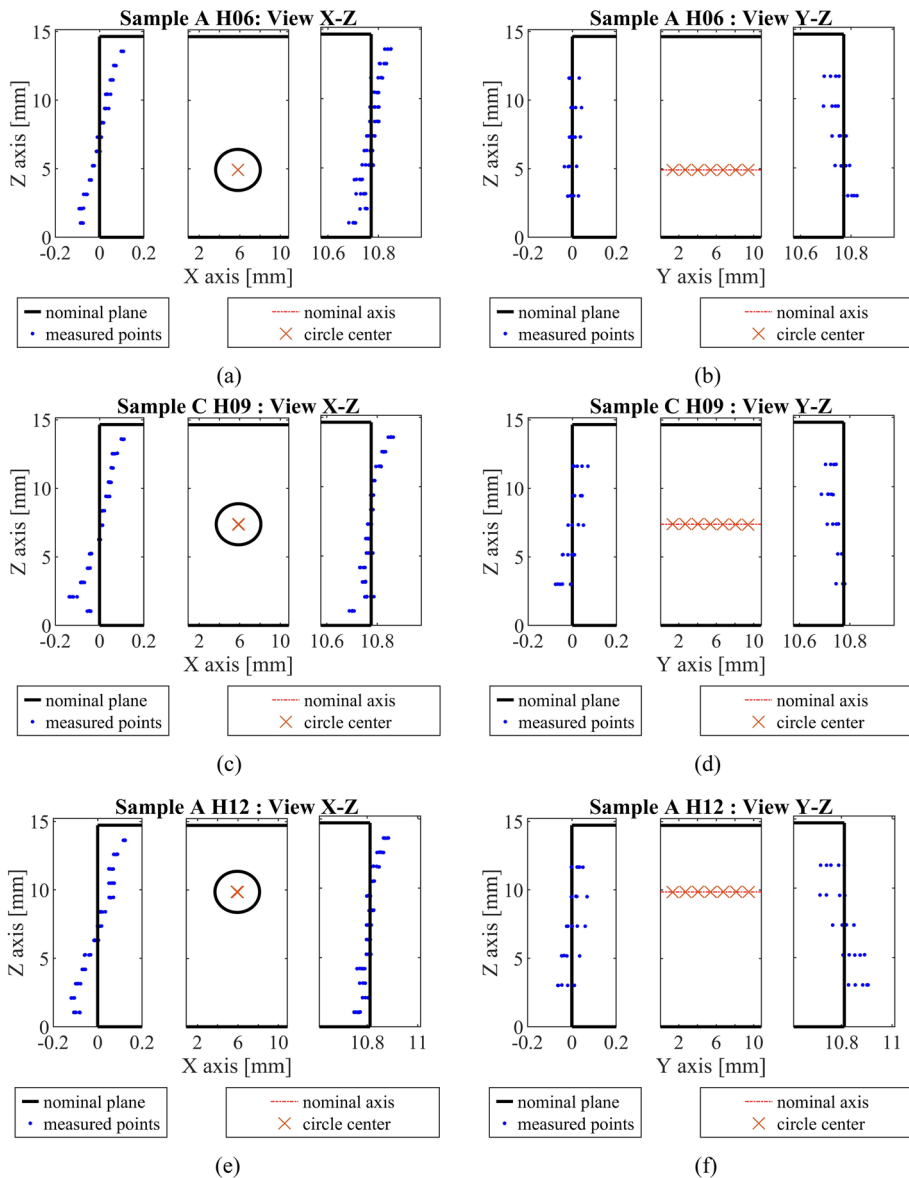
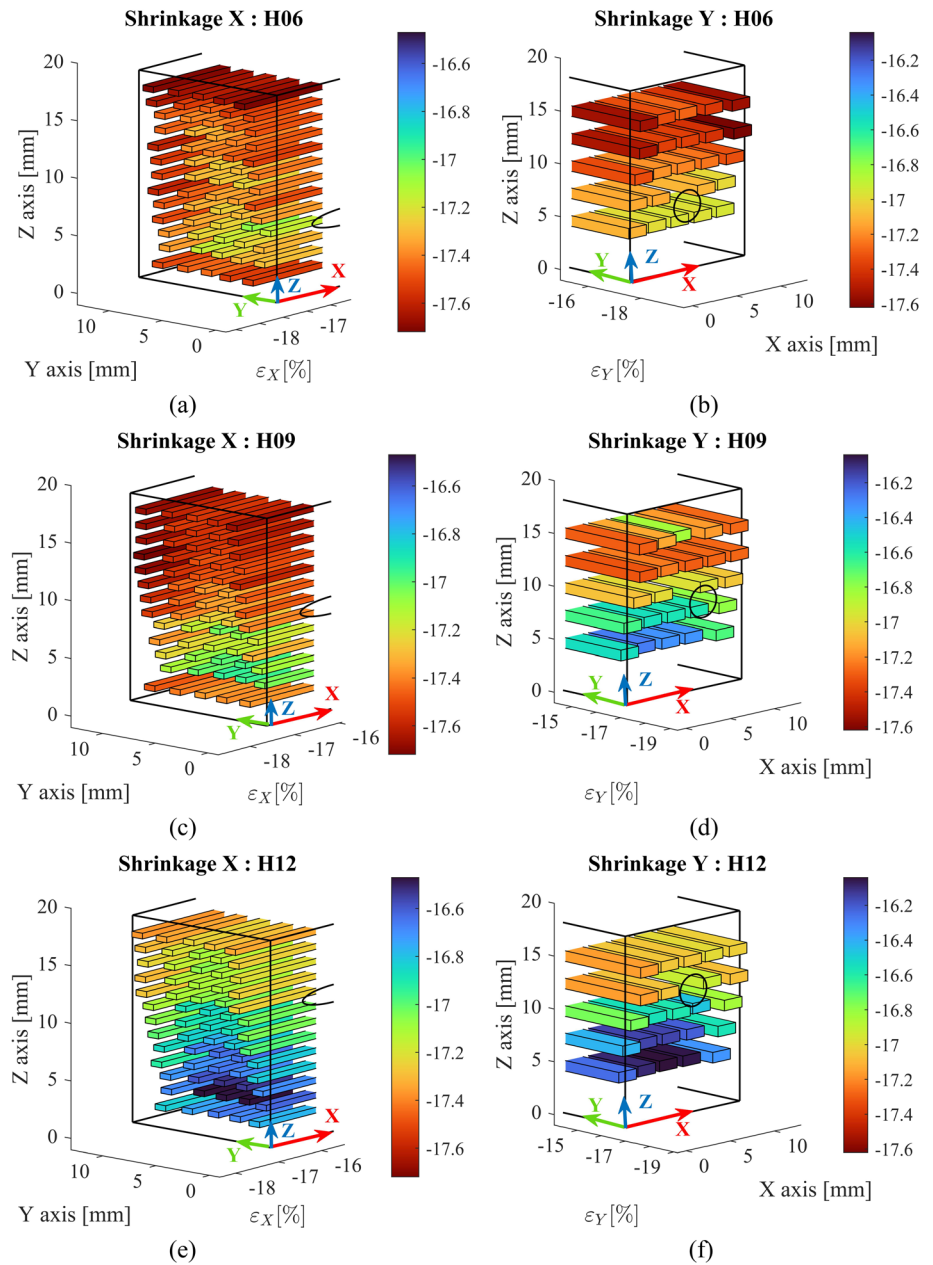


**Fig. 11** Map of the dimensional change on sintering calculated by the distance of points on opposite surfaces. Sample H06—Shrinkage along X direction (a) and shrinkage along Y direction (b); sample H09—Shrinkage along X direction (c) and shrinkage along Y direction (d); sample H12—Shrinkage along X direction (e) and shrinkage along Y direction (f)



jetting process. Three geometries were designed, having a through hole perpendicular to the building direction and located at different position with respect to the building plane.

The linear dimensions and hole diameter were measured by means of a coordinate measuring machine before and after the sintering operation. By this approach, actual dimensional change can be computed as well as shape deformation. Empirical results were then compared with an analytical model previously developed for estimating diameter shrinkage and form error. Main results are following summarized:

- The linear shrinkage is anisotropic, with a significantly higher shrinkage along building direction than in the building plane. In addition, slightly higher shrinkage occurred along printhead movement direction than along powder spreading. The reason is ascribed to an inhomogeneity of powder distribution and binder saturation.
- The linear dimensional changes, and consequently the change in volume, were markedly influenced by sample location in the building plane. Samples located in the center of the building box present marginal fluctuations in the volumetric shrinkage, by contrast parts close to the extreme

positions of printhead highlight appreciably lower shrinkage. The result has been related to a variation in green density.

- The diameter shrinkage of the reconstructed cylinder is not constant, a minimum was detected at the intermediate axis height respect to the building plane. In addition, model prevision considerably underestimated the hole shrinkage for geometries H06 and H12. A tendential decrease in diameters' shrinkage along the hole axis, as well as in circularity form error was also observed, same in the three geometries. Since no trend ascribable to the position of the holes is highlighted, neither for hole shrinkage nor for form error, it can be concluded that the gravity-induced load did not significantly affect the dimensional and geometrical precision in this study.
- Vertical planes showed significant distortion on sintering. Actual sample shape can be represented as a trapezoidal geometry, shifted towards powder spreading direction. The inclination of the planes perpendicular to powder spreading direction might be attributed to the layer shifting originated at green state. The trapezoidal shape is attributed to the frictional forces with support during sintering, determining a gradient of linear shrinkage along sample height.
- The discrepancy between the model prevision and the measurements of hole shrinkage and form error can be attributed to the macroscopic shape distortion of the parallelepiped geometry.

The anisotropic dimensional changes and the distortions highlighted in the present study are largely attributable to the characteristics of the production technology. In principle, any material can show the effect of layer shifting, inhomogeneity of powder distribution/binder saturation, and variations in green density deriving from BJ, and the influence of frictional forces with support related to sintering process. However, the entity and the relative amount of such effects may vary in different materials, both considering the characteristics of powders (powder morphology, size and size distribution), and considering the materials properties. Specifically, materials showing phase transformations determining change in volume can strongly contribute to dimensional changes and distortions, so different materials will be studied in future work.

In conclusion, the design of metal binder jetting parts requires more than correct tuning of the scaling factors in order to compensate the anisotropic shrinkage along 3D directions. The macroscopic distortion must be prevented and correctly counterbalanced in the design of green parts.

**Funding** Open access funding provided by Università degli Studi di Trento within the CRUI-CARE Agreement.

**Open Access** This article is licensed under a Creative Commons Attribution 4.0 International License, which permits use, sharing, adaptation, distribution and reproduction in any medium or format, as long as you give appropriate credit to the original author(s) and the source, provide a link to the Creative Commons licence, and indicate if changes were made. The images or other third party material in this article are included in the article's Creative Commons licence, unless indicated otherwise in a credit line to the material. If material is not included in the article's Creative Commons licence and your intended use is not permitted by statutory regulation or exceeds the permitted use, you will need to obtain permission directly from the copyright holder. To view a copy of this licence, visit <http://creativecommons.org/licenses/by/4.0/>.

## References

1. Dalpadulo, E., Pini, F., Leali, F.: Integrated CAD platform approach for design for additive manufacturing of high performance automotive components. *Int. J. Interact. Des. Manuf.* **14**, 899–909 (2020). <https://doi.org/10.1007/s12008-020-00684-7>
2. Prashar, G., Vasudev, H., Bhuddhi, D.: Additive manufacturing: expanding 3D printing horizon in industry 4.0. *Int. J. Interact. Des. Manuf.* (2022). <https://doi.org/10.1007/s12008-022-00956-4>
3. Ziaee, M., Crane, N.B.: Binder jetting: a review of process, materials, and methods. *Addit. Manuf.* **28**, 781–801 (2019). <https://doi.org/10.1016/j.addma.2019.05.031>
4. Li, M., Du, W., Elwany, A., Pei, Z., Ma, C.: Metal binder jetting additive manufacturing : a literature review. *J. Manuf. Sci. Eng.* **142**, 1–17 (2020). <https://doi.org/10.1115/1.4047430>
5. Crane, N.B.: Impact of part thickness and drying conditions on saturation limits in binder jet additive manufacturing. *Addit. Manuf.* **33**, 101127 (2020). <https://doi.org/10.1016/j.addma.2020.101127>
6. Lores, A., Azurmendi, N., Agote, I., Zuza, E.: A review on recent developments in binder jetting metal additive manufacturing: materials and process characteristics. *Powder Metall.* **62**, 267–296 (2019). <https://doi.org/10.1080/00325899.2019.1669299>
7. Lecis, N., Mariani, M., Beltrami, R., Emanuelli, L., Casati, R., Vedani, M., Molinari, A.: Effects of process parameters, debinding and sintering on the microstructure of 316L stainless steel produced by binder jetting. *Mater. Sci. Eng. A.* **828**, 142108 (2021). <https://doi.org/10.1016/j.msea.2021.142108>
8. Li, M., Du, W., Elwany, A., Pei, Z., Ma, C.: Metal binder jetting additive manufacturing: a literature review. *J. Manuf. Sci. Eng.* **142**, 1–17 (2020). <https://doi.org/10.1115/1.4047430>
9. Bai, Y., Wagner, G., Williams, C.B.: Effect of particle size distribution on powder packing and sintering in binder jetting additive manufacturing of metals. *J. Manuf. Sci. Eng. Trans. ASME.* **139**, 1–15 (2017). <https://doi.org/10.1115/1.4036640>
10. Mostafaei, A., Rodriguez De Vecchis, P., Nettleship, I., Chmielus, M.: Effect of powder size distribution on densification and microstructural evolution of binder-jet 3D-printed alloy 625. *Mater. Des.* **162**, 375–383 (2019). <https://doi.org/10.1016/j.matdes.2018.11.051>
11. Arni, R., Gupta, S.K.: Manufacturability analysis of flatness tolerances in solid freeform fabrication. *J. Mech. Des. Trans. ASME.* **123**, 148–156 (2001). <https://doi.org/10.1115/1.1326439>
12. Paul, R., Anand, S.: Optimal part orientation in Rapid Manufacturing process for achieving geometric tolerances. *J. Manuf. Syst.* **30**, 214–222 (2011). <https://doi.org/10.1016/j.jmsy.2011.07.010>
13. Chen, Q., Xu, J., Zhang, S.: Cylindricity and flatness optimization for mechanical parts in additive manufacturing based on tolerance adaptive slicing. *Int. J. Adv. Manuf. Technol.* **115**, 3839–3857 (2021). <https://doi.org/10.1007/s00170-021-07271-4>

14. Zago, M., Lecis, N., Mariani, M., Cristofolini, I.: Analysis of the flatness form error in binder jetting process as affected by the inclination angle. *Metals* **12**(3), 430 (2022). <https://doi.org/10.3390/met12030430>
15. Miyajima, H., Orth, M., Akbar, J.M., Yang, L.: Process development for green part printing using binder jetting additive manufacturing. *Front. Mech. Eng.* **13**, 504–512 (2018). <https://doi.org/10.1007/s11465-018-0508-8>
16. Cao, S., Qiu, Y., Wei, X.F., Zhang, H.H.: Experimental and theoretical investigation on ultra-thin powder layering in three dimensional printing (3DP) by a novel double-smoothing mechanism. *J. Mater. Process. Technol.* **220**, 231–242 (2015). <https://doi.org/10.1016/j.jmatprotec.2015.01.016>
17. Huang, Z., Dantan, J.Y., Etienne, A., Rivette, M., Bonnet, N.: Geometrical deviation identification and prediction method for additive manufacturing. *Rapid Prototyp. J.* **24**, 1524–1538 (2018). <https://doi.org/10.1108/RPJ-07-2017-0137>
18. Islam, M.N., Sacks, S.: An experimental investigation into the dimensional error of powder-binder three-dimensional printing. *Int. J. Adv. Manuf. Technol.* **82**, 1371–1380 (2016). <https://doi.org/10.1007/s00170-015-7482-7>
19. Ollison, T., Berisso, K.: Three-dimensional printing build variables that impact cylindricity. *J. Ind. Technol.* **26**, 1–10 (2010)
20. Dahmen, T., Klingaa, C.G., Baier-Stegmaier, S., Lapina, A., Pedersen, D.B., Hattel, J.H.: Characterization of channels made by laser powder bed fusion and binder jetting using X-ray CT and image analysis. *Addit. Manuf.* **36**, 101445 (2020). <https://doi.org/10.1016/j.addma.2020.101445>
21. Zago, M., Lecis, N.F.M., Vedani, M., Cristofolini, I.: Dimensional and geometrical precision of parts produced by Binder Jetting process as affected by the anisotropic shrinkage on sintering. *Addit. Manuf.* **43**, 102007 (2021)
22. Zago, M., Lecis, N.F.M., Vedani, M., Cristofolini, I.: Geometrical Issues in Design for Binder Jetting – The Effect of Anisotropic Dimensional Change on Sintering. In: Rizzi, C., Campana, F., Bici, M., Gherardini, F., Ingrassia, T., Cicconi, P. (eds.) *Des Tools Methods Ind. Eng. II*, pp. 410–421. Springer International Publishing, Cham (2022)
23. Zhang, K., Zhang, W., Brune, R., Herderick, E., Zhang, X., Cornell, J., Forsmark, J.: Numerical simulation and experimental measurement of pressureless sintering of stainless steel part printed by Binder Jetting Additive Manufacturing. *Addit. Manuf.* **47**, 102330 (2021). <https://doi.org/10.1016/j.addma.2021.102330>
24. Sadeghi Borujeni, S., Shad, A., Abburi Venkata, K., Günther, N., Ploshikhin, V.: Numerical simulation of shrinkage and deformation during sintering in metal binder jetting with experimental validation. *Mater. Des.* **216**, 110490 (2022). <https://doi.org/10.1016/j.matdes.2022.110490>
25. Paudel, B.J., Conover, D., Lee, J.K., To, A.C.: A computational framework for modeling distortion during sintering of binder jet printed parts. *J. Micromechanics Mol. Phys.* **6**, 95–102 (2021). <https://doi.org/10.1142/S242491302142008X>
26. Vitolo, F., Martorelli, M., Gerbino, S., Patalano, S., Lanzotti, A.: Controlling form errors in 3D printed models associated to size and position on the working plane. *Int. J. Interact. Des. Manuf.* **12**, 969–977 (2018). <https://doi.org/10.1007/s12008-017-0441-9>
27. Ziaee, M., Tridas, E.M., Crane, N.B.: Binder-Jet Printing of Fine Stainless Steel Powder with Varied Final Density. *Jom.* **69**, 592–596 (2017). <https://doi.org/10.1007/s11837-016-2177-6>
28. Wakai, F., Chihara, K., Yoshida, M.: Anisotropic shrinkage induced by particle rearrangement in sintering. *Acta Mater.* **55**, 4553–4566 (2007). <https://doi.org/10.1016/j.actamat.2007.04.027>
29. Huber, D., Vogel, L., Fischer, A.: The effects of sintering temperature and hold time on densification, mechanical properties and microstructural characteristics of binder jet 3D printed 17–4 PH stainless steel. *Addit. Manuf.* **46**, 102114 (2021). <https://doi.org/10.1016/j.addma.2021.102114>
30. Rios, A.C., Hryha, E., Olevsky, E., Harlin, P.: Sintering anisotropy of binder jetted 316L stainless steel: part I – sintering anisotropy. *Powder Metall.* **65**(4), 273–282 (2021). <https://doi.org/10.1080/00325899.2021.2020485>
31. Lores, A., Azumendi, N., Agote, I., Andres, U.: A step towards a robust binder jetting technology: Process parameter optimization for 17–4 PH steel to increase powder bed homogeneity. In: *Proceedings Eur. 2020 Int. Powder Metall. Virtual Congr. Exhib.* (2020).
32. Do, T., Shin, C.S., Stetsko, D., Vanconant, G., Vartanian, A., Pei, S., Kwon, P.: Improving Structural integrity with boron - based additives for 3D printed 420 stainless steel. *Procedia Manuf.* **1**, 263–272 (2015). <https://doi.org/10.1016/j.promfg.2015.09.019>
33. Chen, Z., Chen, W., Chen, L., Zhu, D., Chen, Q., Fu, Z.: Influence of initial relative densities on the sintering behavior and mechanical behavior of 316 L stainless steel fabricated by binder jet 3D printing. *Mater. Today Commun.* **31**, 103369 (2022). <https://doi.org/10.1016/j.mtcomm.2022.103369>
34. Maximenko, A.L., Olumor, I.D., Maidaniuk, A.P., Olevsky, E.A.: Modeling of effect of powder spreading on green body dimensional accuracy in additive manufacturing by binder jetting. *Powder Technol.* **385**, 60–68 (2021). <https://doi.org/10.1016/j.powtec.2021.02.070>
35. Olevsky, E.A., German, R.M., Upadhyaya, A.: Effect of gravity on dimensional change during sintering - II Shape distortion. *Acta Mater.* **48**, 1167–1180 (2000). [https://doi.org/10.1016/S1359-6454\(99\)00369-9](https://doi.org/10.1016/S1359-6454(99)00369-9)

**Publisher's Note** Springer Nature remains neutral with regard to jurisdictional claims in published maps and institutional affiliations.